Vertically aligned Ni/NiO nanocomposites with abundant oxygen deficient hetero-interfaces for enhanced overall water splitting

Hongxia Wang, Meiyan Cui, Gaoliang Fu, Jiaye Zhang, Xingyu Ding, Irene Azaceta, Matthieu Bugnet, Demie M. Kepaptsoglou, Vlado K. Lazarov, Victor A. de La Pena O'Shea, et al.

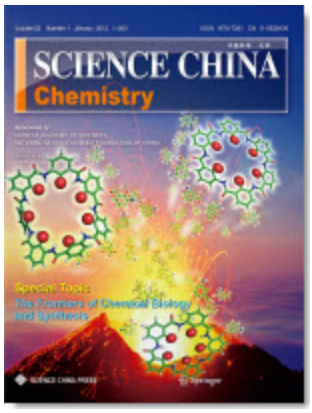

Vertically Aligned Ni/NiO Nanocomposites with Abundant Oxygen Deficient Hetero-interfaces for Enhanced Overall Water Splitting

Journal:	*SCIENCE CHINA Chemistry*
Manuscript ID	SCC-2022-0551.R1
Manuscript Type:	Article
Date Submitted by the Author:	01-Jul-2022
Complete List of Authors:	Zhang, Kelvin H.L. Wang, Hongxia Cui, Meiyan Fu, Gaoliang Zhang, Jiaye Ding, Xingyu Azaceta, Irene Bugnet, M. Kepaptsoglou, Demie Lazarov, Vlado VAD , O'Shea Oropeza, Freddy
Keywords:	Water splitting, Hydrogen evolution reaction, Electronic structure, Heterostructure, Vertically aligned nanocomposites
Speciality:	Inorganic Chemistry

Vertically Aligned Ni/NiO Nanocomposites with Abundant Oxygen Deficient Hetero-interfaces for Enhanced Overall Water Splitting

Hongxia Wang[1#], Meiyan Cui[2#], Gaoliang Fu[1,3], Jiaye Zhang[1], Xingyu Ding[1], Irene Azaceta[4], M. Bugnet[5,6,7], Demie M. Kepaptsoglou[4,5], Vlado K. Lazarov[4], Victor de la Peña O'Shea[8], Freddy E. Oropeza[8*], and Kelvin H. L. Zhang[1*]

[1]*State Key Laboratory of Physical Chemistry of Solid Surfaces, College of Chemistry and Chemical Engineering, Xiamen University, Xiamen 361005, P. R. China*

[2]*State Key Laboratory of Structural Chemistry, Fujian Institute of Research on the Structure of Matter, Chinese Academy of Sciences, Fuzhou 350002, P. R. China*

[3]*Henan Provincial Key Laboratory of Nanocomposites and Applications, Institute of Nanostructured Functional Materials, Huanghe Science and Technology College, Zhengzhou, Henan 450006, China*

[4]*Department of Physics, University of York, Heslington, York, YO10 5DD, U. K.*

[5]*SuperSTEM Laboratory, SciTech Daresbury Campus, Daresbury WA4 4AD, United Kingdom*

[6]*School of Chemical and Process Engineering, Univeristy of Leeds, Leeds LS2 9JT, United Kingdom*

[7]*Univ Lyon, CNRS, INSA Lyon, UCBL, MATEIS, UMR 5510, 69621 Villeurbanne, France*

[8]*Photoactivated Processes Unit, IMDEA Energy Institute, Parque Tecnológico de Móstoles, Avda. Ramón de la Sagra 3, 28935 Móstoles, Madrid, Spain.*

[#]Equal Contribution

Email: freddy.oropeza@imdea.org; kelvinzhang@xmu.edu.cn

Abstract:

The design of heterostructured transition metal-based electrocatalysts with controlled composition and interfaces is key to increasing the efficiency of the water electrolysis and the elucidation of reaction mechanisms. In this work, we report the synthesis of well-controlled vertically aligned Ni/NiO nanocomposite consisting of Ni nanoclusters embedded in NiO, which result in highly efficient electrocatalysts for overall water splitting. We show that such high catalytic efficiency toward both the hydrogen evolution reaction (HER) and the oxygen evolution reaction

https://engine.scichina.com/doi/10.1007/s11426-022-1326-2
http://chem.scichina.com/english

(OER) originates from a synergetic effect at Ni/NiO interfaces that significantly reduces the energy barrier for water dissociation, and favors the formation of reactive H* intermediates on the Ni side of the interface, and OH_{ads} on the NiO side of the interface. A study of water chemisorption based on near-ambient pressure photoelectron spectroscopy indicates that the abundant hetero-interfaces in Ni/NiO nanocomposite promote the dissociation of water with a three-fold increase in the surface concentration of OH_{ads} compared with pure NiO. Density functional theory calculations indicate that Ni/NiO interface leads to the reduction of water dissociation energy barrier due to a high concentration of oxygen vacancies at NiO side of the interface, whereas the formation of highly active metallic Ni sites with an optimal value of Gibbs free energy of H* (ΔG_{H^*}=-0.16 eV) owes to a favorable adjustment of the electron energetics at the interface, thus accelerating the overall electrochemical water splitting.

Keywords: Water splitting; Hydrogen evolution reaction; Electronic structure; Heterostructure; Vertically aligned nanocomposites

1. Introduction

Electrolysis of water powered by renewable electricity to produce hydrogen is widely considered as a promising pathway for global clean and sustainable energy supply in the future.[1-4] The key to enable this technology is the development of low-cost and efficient electrocatalysts with enhanced activity and stability to accelerate the water splitting reactions, *i.e.*, hydrogen evolution reaction (HER) and oxygen evolution reaction (OER).[5] At present, the most effective HER and OER electrocatalysts are Pt/Pd and RuO_2/IrO_2 based materials, respectively.[6-11] Although these noble metal based catalysts exhibit high performance, their large-scale applications are limited by high costs and scarcity. Therefore, great efforts have been devoted to investigate earth-abundant transition metals (Co, Ni, Fe) based materials.[12-14] However, most of them generally perform well only for the half-cell reaction (either HER or OER) in either alkaline or acidic media.[15, 16] Therefore, developing highly efficient bifunctional electrocatalysts which can simultaneously catalyze HER and OER process in the same electrolyte, is technologically crucial to increase the overall efficiency of water electrolysis.

Up to now, there are two mature water electrolysis systems: proton exchange membrane water electrolyser (PEMWE) performed in acidic condition, and alkaline water electrolyser (AWE)

https://engine.scichina.com/doi/10.1007/s11426-022-1326-2
http://chem.scichina.com/english

worked in alkaline media.[17] PEMWE has the advantages of high current densities, high efficiency and high gas purity. However, it faces problem with the scaling-up due to the high cost of the components like Pt/Pd and RuO_2/IrO_2 based electrocatalyst materials.[18] To this regard, AWE electrolyser, which utilizes low-cost transition metal-based catalysts, is more appealing for large-scale industrialization. Additionally, in alkaline media, most OER catalysts show faster reaction kinetics and better stability compared to those in acidic solution. However, so far the alkaline HER still suffers from sluggish reaction kinetics due to the additional water dissociation step, which decreases the efficiency of the overall process. Even for Pt, the HER performance in alkaline condition is limited by slow water dissociation due to the lack of optimal active sites for H-OH bond cleaving.[19, 20] Motivated by this, designing active bifunctional catalysts capable of appropriate adsorption and transformation of hydrogen and oxygen involved intermediates for both OER and HER in alkaline media is highly desirable. Encouragingly, some studies reveal that multifunctional heterojunctions could accelerate the water dissociation step and achieve high intrinsic activity in alkaline media. For example, Subbaraman *et al* proposed Pt/$Ni(OH)_2$ heterostructured catalyst with outstanding HER performance, in which the $Ni(OH)_2$ clusters promote water dissociation, and Pt serves as the active site to generate molecular hydrogen.[21] Subsequently, considerable research efforts have been devoted to investigating heterostructure catalysts, which show superior multifunctional catalytic activities for HER, OER or both.[22, 23] For instance, Xie and co-workers reported a Fe_3O_4-blended Ni/NiO heterostructure catalyst, exhibiting high performance toward both OER and HER, due to the synergetic effects between Ni/NiO compound and Fe_3O_4.[24] Although recent advances in nanostructured materials have led to the development of high-performance catalysts for HER and OER, the real active sites and reaction mechanism are still ambiguous.[25, 26]

Most of the previously reported heterostructured catalysts are based on nanostructures with different morphologies, exposed crystal facets, and defects, which would complicate the elucidation of possible active sites and the reaction mechanism.[27, 28] Recently, vertically aligned nanocomposites (VAN),[29, 30] which possess two or more epitaxially grown phases on substrates, open up new possibilities for the design of heterostructured catalysts.[31] VAN materials provide abundant well-defined hetero-interface on the surface with precise control over the crystal

https://engine.scichina.com/doi/10.1007/s11426-022-1326-2
http://chem.scichina.com/english

orientation, roughness and thickness, therefore avoiding structural and morphological ambiguity inherent to the preparation of free standing powder catalysts.[32, 33] Such VAN catalysts can provide ideal platforms to characterize the structural and electronic properties of multifunctional heterostructures, and to study the reaction mechanism. In addition, VAN can also significantly enhance the electrical conductivity to boost overall water splitting performance owing to the strong interfacial interaction between the components of the composite and the substrate, which minimizes issues of phase segregations and mechanical peeling of active components. Although VAN have been used as model catalysts for several chemical reactions, they are rarely applied for electrochemical water splitting.

In this work, we show that Ni/NiO VAN are efficient catalyst for both the alkaline HER and OER, owing to synergetic effect at the Ni/NiO interface that significantly reduce the energy barrier for water dissociation, and favors the formation of reactive key H* intermediates on the Ni side of the interface, and OH_{ads} on the NiO side of the interface. For our study, vertically aligned Ni/NiO nanocomposite catalysts on the conductive (001) oriented Nb-doped $SrTiO_3$ (Nb:STO) substrates were prepared using pulsed laser deposition (PLD). Different from previously reported Ni-based heterostructure catalysts that are prepared by hydrothermal,[34] electrodeposition[35] or thermal annealing[36] methods, the vertically aligned Ni/NiO heterostructure is grown by a self-decomposition thin-film growth mechanism, in which the metallic Ni phase is segregated from NiO matrix, resulting in nanocomposite with abundant Ni/NiO heterointerfaces. Compared with individual Ni and NiO, the Ni/NiO VAN prepared this way show enhanced HER and OER performance in alkaline media. A study of water absorption based on near-ambient pressure X-ray photoelectron spectroscopy (NAP-XPS) shows that the enhanced catalytic performances are correlated with a substantial increase of the water dissociation capability of Ni/NiO VAN. Based on density-functional theory (DFT) calculations, we propose that the existence of oxygen vacancies at the interface of Ni/NiO VAN promotes the water dissociation and adsorption of OH_{ads}. This work reveals insights into the mechanism of Ni/NiO heterostructure for overall water splitting, and provide an effective strategy for the design of novel heterostructure catalysts with well-defined interface.

2. Experimental Section

2.1. Thin films growth.

NiO and Ni/NiO VAN thin films were epitaxially grown on Nb:STO(001) substrates by PLD with a 248 nm KrF excimer from NiO target at the oxygen partial pressure of 10 and 0.01 mTorr, respectively. The NiO target was made from NiO powder (99.998%, Alfa Aesar) by pelletizing and sintering in air at 1100 °C for 12 hours. During the growth of NiO, the laser repetition rate and energy density, and the substrate temperature were set as 5 Hz, 1.2 J cm^{-2} and 600 °C, respectively. Ni thin films on Nb:STO(001) substrates were synthesized via magnetron sputtering with a thickness of ~50 nm. Sputtering was performed at a rf power of 200 W and the Ar pressure of 3.8 mTorr for direct deposition from a Ni target.

2.2. Characterizations.

The crystal structure of NiO, Ni/NiO VAN and Ni was examined by high-resolution XRD using a PANalytical four-circle diffractometer in θ-2θ scans and reciprocal space mapping modes. Atomic force microscopy (AFM) with tapping-mode was applied to characterize surface morphologies. The detailed structure of Ni and Ni/NiO VAN were characterized by scanning transmission electron microscopy (STEM) and electron energy-loss spectroscopy (EELS) measurements, performed in a Nion UltraSTEM100 equipped with a Gatan Enfina spectrometer and a Nion UltraSTEM100MC monochromated instrument equipped with a Gatan Enfinium spectrometer. Both instruments were operated at 100kV, with electron optics set to form a 0.9 Å probe. Cross-sectional transmission electron microscopy (TEM) specimen preparation was carried out by focused ion beam (FIB) milling using an FEI Helios NanoLab 600 instrument. The x-ray absorption spectroscopy (XAS) spectra were conducted under the total electron yield (TEY) mode with an effective resolution of 0.2 eV at the I09 Surface and Interface Structural Analysis beamline of the Diamond Light Source (DLS). And X-ray adsorption near edge structure (XANES) measurements at the Ni K edges were performed at the XAFCA beamline of Singapore Synchrotron Light Source (SSLS). X-ray photoemission spectroscopy (XPS) were characterized by a monochromatic Al Kα X-ray (hυ= 1486.6 eV) source at normal emission (electron take-off angle=90º relative to the surface plane) with a SPECS PHOIBOS 150 electron energy analyzer. Near ambient pressure XPS spectra were obtained through a lab-based spectrometer with a monochromated Al Kα source. A SPECS

https://engine.scichina.com/doi/10.1007/s11426-022-1326-2
http://chem.scichina.com/english

PHOIBOS 150 NAP analyser was used. The entrance to the analyser is a nozzle with a 300 mm diameter orifice. The total energy resolution of the measurements was about 0.50 eV.

2.3. Electrochemical analysis.

The NiO, Ni/NiO VAN and Ni thin film electrodes were prepared by the method previously reported. Nb:STO substrates are conductive so that the electrical contact attached to a narrow copper stripe was made to the back of the NiO, Ni/NiO VAN and Ni thin films (instead of the front of thin films) using GaIn eutectic and Ag paste. The sides of thin films and copper stripe were covered with epoxy. The catalyst surface is calculated according to the actual exposed surface area. The CHI 660E electrochemical workstation was used for the electrochemical measurements for OER in 0.1M KOH using a typical three-electrode system. A Hg/HgO (0.1 M KOH) electrode and carbon rob were worked as the reference electrode and counter electrode, respectively. The electrolyte was prepared by high-purify KOH (Adamas, 99.999%) and Milli-Q water (18.2 MΩ-cm). In order to detach the impurity on the surface of electrode, cyclic voltammograms (CV) were firstly performed under the potential range of 0 to 0.60 V (vs RHE). Then, linear sweep voltammetry (LSV) polarization curves for OER were carried out with the potential range of -0.1 to 0.8 V (vs Hg/HgO) at a scan rate 10 mV s−1. The electrochemical impedance spectroscopy (EIS) measurement was conducted from 100 kHz to 1 Hz at a potential of 0.7 V (vs Hg/HgO). All potential values were converted to reversible hydrogen electrode (RHE) according to the Nernst equation: $E_{RHE} = E_{Hg/HgO} + 0.059\ pH + 0.164\ V$.

3. Results and Discussion

3.1. Synthesis of vertically aligned Ni/NiO heterointerfaces

To realize the growth of two phases, the PLD growth was conducted at a low oxygen partial pressure of 0.1 mTorr. Similar to the growth process of other self-assembled nanocomposites,[37] the growth of Ni/NiO VAN may go through a three-stage self-decomposition mechanism.[38] In the first stage, NiO adatoms vaporized from NiO target nucleate on the Nb:STO substrate. During the deposition process, a low oxygen pressure triggers the phase segregation of Ni from NiO to form ultra-fine Ni clusters. Next, thermal energy facilitates the coalescence of Ni clusters, forming Ni nanodomains. In the third stage, the phase segregation is stabilized, leading to a vertically aligned

https://engine.scichina.com/doi/10.1007/s11426-022-1326-2
http://chem.scichina.com/english

heterostructure. In addition, NiO and metallic Ni thin films were also prepared as reference samples (see details in the Experimental Section).

Figure 1a presents XRD θ-2θ scans for NiO, Ni/NiO VAN and Ni thin films. Sharp Bragg peaks at 43.2° and 51.8° corresponding to NiO (002) and metallic Ni (002), respectively, are observed in the scan of Ni/NiO VAN, indicating the formation of Ni/NiO heterostructures. To gain additional structural information, reciprocal space maps (RSMs) of NiO and Ni/NiO VAN near the (113) reflection of Nb:STO were measured (as shown in Figure 1b and c), from which the in-plane and out-of-plane lattice parameters were extracted. According to the lattice parameters, the unit cell volume can be calculated. As displayed in Figure S1, the unit cell volume of NiO in Ni/NiO VAN is larger than that of pure NiO. The expansion of unit cell volume of NiO in Ni/NiO VAN may be caused by the generation of oxygen vacancies at the Ni/NiO interface.[39, 40]

Cross-sectional STEM images were collected to further investigate microscopic structure. Figure 1 d and e show the large-scale cross-sectional STEM images of NiO and Ni/NiO VAN. Different from the continuous flat layer observed in the NiO film, the image of Ni/NiO VAN has brighter regions of metallic Ni due to the high Ni concentration.[38] Metallic Ni and NiO phases coexist with a fairly uniform distribution of Ni clusters of 20~30 nm embedded in NiO matrix. The HAADF-STEM image and corresponding energy-dispersive X-ray spectroscopy (EDX) elemental maps on the sample region are shown in Figure 1f. We can see that the Ni-NiO coupling leads to a single crystalline stacking and distinctive interface between Ni and NiO. The high-resolution HAADF-STEM image (Figure 2g and h) near the Nb:STO substrate viewed along the Nb:STO [-1-10] direction, shows the epitaxial growth of the two crystalline phases. The lattice plane spacing in the Ni domain near the interface, 2.08 Å and 2.35 Å, correspond to Ni(002) and Ni(-111), respectively. In the NiO domain, lattice plane spacing of 2.14 Å and 2.35 Å correspond to NiO (002) and NiO (-111), respectively. The difference in lattice parameter between Ni and NiO results in a 3% lattice mismatch at the Ni/NiO interface, which may lead to the generation of oxygen vacancies at the Ni/NiO interface.[41]

The chemical compositions of NiO, Ni/NiO VAN and Ni were studied by XAS and XPS. Figure 2a shows the XANES)at the Ni-K edge of each sample. The pre-edge peak at ~8330 eV is assigned to the electron transition of 1s to 3d state,[42] which is observed in NiO, but absent in metallic

https://engine.scichina.com/doi/10.1007/s11426-022-1326-2
http://chem.scichina.com/english

Ni.[43] Metallic Ni exhibits a pre-edge peak at ~8332 eV. The enhancement of this pre-edge peak can be regarded as an indication of the existence of metallic Ni. For Ni/NiO VAN, the pre-edge peak at ~8332 eV can also be observed, indicating that both NiO and metallic Ni presented in Ni/NiO film. This could be further supported by the line-shape of Ni 2p XPS of Ni/NiO VAN, shown in Figure 2b, which exhibits spectral feature associated with both NiO in the range of 855~858 eV, and metallic Ni at around 853.0 eV (see Ni 2p XPS of pure Ni and NiO in Figure S2). Figure S3 shows the O 1s spectra of Ni/NiO VAN, NiO and Ni. The O 1s spectra of Ni/NiO VAN and NiO are deconvoluted into three peaks that represent contributions from three oxygenated species, including lattice oxygen (O_{Latt}) at ~529.6 eV, defective oxygen at ~531.1 eV (V_o), adsorbed OH groups (OH_{ads}) at ~532.3 eV, while the O 1s spectrum of Ni only shows a weak peak assigned to the adsorbed OH groups.[44, 45] The percentage of V_o shows a high value (35.4 %) for the Ni/NiO VAN, proving the existence of abundant oxygen vacancies in the Ni/NiO VAN.

In order to investigate the chemical and electronic information of the Ni/NiO VAN interface, high energy-resolution EELS was conducted in the three regions (as shown in Figure 2c), including the Ni region (blue box), the region of Ni/NiO interface (pink box) and the NiO region (gray box). The Ni-L_2 and -L_3 edges, due to the electronic transition from $2p_{1/2}$ and $2p_{3/2}$ to unoccupied 3d state, are highly sensitive to changes in the occupancy of d states.[46] The energy position, sub-splitting of the L_3 and L_2 peaks, as well as their relative intensity ratio can be related to the valence state and O coordination of Ni.[47, 48] Comparing the fine structures of Ni-L edges in the three regions marked in Figure 2d, a clear change of the near edge fine structure can be observed as we scan from the NiO to the Ni/NiO and Ni regions: (1) the sub-splitting of the L_3 (high energy shoulder) and L_2 (doublet) peaks gradually decrease; (2) the splitting is accompanied by a gradual shift of the edge onset towards lower energies; (3) there is a decrease of the L_3/L_2 intensity ratio. These changes suggest the presence of unsaturated coordinated Ni atoms at the Ni/NiO interface.[49, 50] The results obtained from the Ni-$L_{2,3}$ fine structures are further confirmed by the analysis of O-K edge spectra. As is shown in Figure 2e, peak A at ~530 eV arises from the electronic transition from O 1s to unoccupied state with partial O 2p character hybridized with empty Ni 3d states.[51] Peak C at ~540 eV and peak D at ~550 eV correspond to the electronic transition from O 1s to the hybridization orbital of O 2p with Ni 4s and 4p, respectively.[52] The origin of peak B can be ascribed to the

https://engine.scichina.com/doi/10.1007/s11426-022-1326-2
http://chem.scichina.com/english

multi-electron configuration interaction.[53] Therefore, the density of O-K edge is related to the oxygen coordination and the Ni oxidation state. It can be seen that the O-K edge of the NiO region exhibits sharp A–D peaks, while at the Ni/NiO interface, the relative intensity of peaks B and C become weaker, while a slight redshift of the edge onset can also be observed. These results can be assigned to the breaking of long range order and further indicate the presence of oxygen vacancies at the Ni/NiO interface.[51] Oxygen vacancies at the NiO side of the interface (Figure 2f) result in the unsaturated coordinated coordination Ni atoms and a higher *d* band occupancy of Ni due to the nominal electron density donation from oxygen vacancies to the Ni cations.

3.2. Electrocatalytic Performance

The HER and OER activities of NiO, Ni/NiO VAN and Ni thin films were evaluated in a standard three-electrode setup in 0.1 M KOH solution, which have been commonly used for model thin film electrocatalysts.[54-56] Figure 3a presents the first linear sweep voltammetry (LSV) curves for the HER for each sample. The Ni/NiO VAN delivers the best HER catalytic performance. As shown in Figure 3b, the Ni/NiO VAN requires a low overpotential of 0.196 V to reach 10 μA cm^{-2}, which is significantly lower than the overpotentials of metallic Ni (0.302 V) and NiO (0.420 V). To understand the kinetics of HER, the corresponding Tafel plots are calculated from the linear region of the polarization curves. It is widely accepted that Tafel slopes values around 120, 40 and 30 mV dec^{-1} are observed when the alkaline HER rate is determined by the Volmer, Heyrovsky and Tafel steps, respectively. As shown in Figure 3c, the Tafel slopes of the HER for all electrode samples have values above 100 mV dec^{-1}, suggesting that Volmer step (the water dissociation step) is the rate-determining step for the reaction driven by all studied catalyst. However, the Tafel slope of Ni/NiO VAN has a significantly smaller value (108 mV dec^{-1}) than that for the HER driven by metallic Ni (156 mV dec^{-1}) and NiO (238 mV dec^{-1}), which means a faster Volmer step and a higher hydrogen generation rate for Ni/NiO VAN. Furthermore, the electrochemical impedance spectroscopy (EIS) was conducted to investigate the electron-transfer HER kinetics. As shown in Figure S4, the charge transfer resistance (R_{ct}) for Ni/NiO VAN (290.4 Ω) is smaller than that of Ni (516.1 Ω) and NiO (3708.8 Ω), indicating the faster Faradaic process and HER kinetics of Ni/NiO VAN. The stability of samples was also measured by chronopotentiometry. As displayed in Figure S5, the potentials of all samples maintained a constant current density of -20 μA cm^{-2} don't exhibit

https://engine.scichina.com/doi/10.1007/s11426-022-1326-2
http://chem.scichina.com/english

obvious change during the continuous electrolysis for 10 hours, indicating the good stability of three catalysts.

The OER catalytic performance of NiO, Ni/NiO VAN and Ni was also investigated in 0.1 M KOH solution. The LSV curves (Figure 3d) revealed that Ni/NiO VAN presents a much larger catalytic current density and lower onset potential than those of Ni and NiO. As shown in Figure 3e, in order to reach a current density of 10 μA cm^{-2}, the overpotential required with Ni/NiO VAN is 0.164 V, which is significantly lower than that needed with Ni (0.371 V) and NiO (0.310 V). The Tafel slopes of Ni/NiO VAN, Ni and NiO are 88, 93 and 116 mV dec^{-1}, respectively, further indicating a favorable OER kinetics for Ni/NiO VAN (Figure 3f). In addition, the electron-transport kinetics of OER are studied by EIS. From the Nyquist plots of Ni/NiO VAN, Ni and NiO (Figure S6), the R_{ct} value of Ni/NiO VAN is smaller compared with NiO and Ni, indicating a faster Faradaic process and OER kinetics of the Ni/NiO VAN catalyst. Moreover, we also conducted stability measurement. The chronopotentiometric curves shown in Figure S7 suggest the high stability of the catalyst owing to no significant change of the OER performance during the continuous electrolysis at 20 μA cm^{-2} for 10 hours.

To investigate the electrochemically active surface areas (ECSA) of the samples, CV measurement was performed to obtain the double layer capacitance (C_{dl}). As shown in Figure S8, the Ni/NiO VAN shows the highest C_{dl} value (46.8 μF cm^{-2}) compared with Ni (17.3 μF cm^{-2}) and NiO (25.6 μF cm^{-2}), thereby suggesting the highest catalytically relevant surface area. However, in the HER process, Ni shows better performance than NiO, which is not consistent with the trend of C_{dl} values. Thus, this approach used for determining the ECSA is limited. Moreover, the C_{dl} can be affected by several factors, such as the conductivity, the surface coordination of ions, and capacitance originated from the trap states and residual charge-transfer processes in non-Faradaic region.[57, 58] Thus, the ECSA obtained by C_{dl} may not reflect the real active area of electrocatalysts and can serve as an additional parameter for the performance indication.

Inspired by the good HER and OER performance of Ni/NiO VAN, we use Ni/NiO VAN as both the anode and cathode to assemble an electrolyzer for overall water splitting in alkaline condition. For comparison, NiO and Ni catalysts were also used to assemble the alkaline electrolyzer. The LSV curves of Ni/NiO VAN‖Ni/NiO VAN, Ni‖Ni and NiO‖NiO are presented in Figure S9. It can be seen

https://engine.scichina.com/doi/10.1007/s11426-022-1326-2
http://chem.scichina.com/english

that Ni/NiO VAN only requires a low cell voltage of 1.59 V to deliver a current density of 10 μA cm^{-2}, which is smaller than that of Ni (1.68 V) and NiO (1.87 V). The better water splitting performance of Ni/NiO VAN is ascribed to the synergetic effect at Ni/NiO interfaces.

3.3. Mechanism Study: Origin of Enhanced OER and HER Performance

As revealed by the electrocatalytic performance tests, Ni/NiO VAN interface seems to favor the Volmer step, *i.e.*, the water dissociation, during the HER process. To better understand the adsorption and dissociation of water on the Ni/NiO heterostructure, we investigated the reactivity of water vapor on Ni/NiO VAN and NiO surfaces using NAP-XPS. In the experiment, we monitored the O 1s region of the spectra of the sample as water vapor was dosed into the chamber at pressures ranging from 7×10^{-7} mbar to 2.5 mbar. Figure 4a shows photoelectron spectra of Ni/NiO VAN and NiO in the O 1s region under vacuum and 0.6 mbar water vapor pressure (see supplementary Figure S10 for other water pressure). The spectra can be fitted with four curves that represent contributions from four oxygenated species, including lattice oxygen at ~530 eV, adsorbed OH groups at ~531.8 eV, chemisorbed H_2O (H_2O_{ads}) at ~533.2 eV, and gaseous H_2O (H_2O_{gas}) at ~535 eV,[59, 60] and their relative amounts can be obtained from peak fit area (Figure 4b). In particular, the absorbed OH* originates from the dissociative H_2O, and therefore can be used as a measure of the degree of water dissociation on catalyst surface, *i.e.*, the higher the value, the better the ability to dissociate water. Figure 5b shows plots of the percentage of adsorbed hydroxyl as a function of water vapor pressure. The percentage of OH_{ads} content remains within 15-25 % for NiO under different water pressure, but OH_{ads} content increases dramatically up to ~50 % for Ni/NiO VAN. The considerable increase of the hydroxylation on the Ni/NiO surface suggests that the dissociative adsorption of water is more favorable on Ni/NiO surface, and thereby accelerates the Volmer step which is the rate determining step for the HER process in alkaline conditions. At the surface with oxygen vacancies, the undercoordinated metal centers near oxygen vacancies are more active towards the adsorption of H_2O and OH to achieve a saturated coordination than that at the surface without oxygen vacancies.[5] Therefore, we propose that the oxygen vacancies existed at Ni/NiO interface may promote the observed dissociative adsorption of H_2O to form chemisorbed OH_{ads} and H_{ads} (as shown in Figure 4c), also can promote the adsorption of OH_{ads} on the catalyst surface, which contributes to the highly enhanced electrocatalytic activity for the both OER and HER.

https://engine.scichina.com/doi/10.1007/s11426-022-1326-2
http://chem.scichina.com/english

3.4. DFT Calculations.

To clarify the role of Ni/NiO hetero-interface on the adsorption of reaction intermediates and the enhanced catalytic activity, DFT calculations were employed to evaluate the energy barrier for breaking the H-OH bond in H_2O and the chemisorption free energies of hydrogen (ΔG_{H^*}) on the (001) surface of pure Ni, pure NiO, Ni/NiO VAN, and Ni/NiO without oxygen vacancy (denoted as w/o-Ni/NiO). The structure models are shown in Figure S11. As shown in Figure S12, the energy barriers of pure Ni, pure NiO and w/o-Ni/NiO (001) surface for breaking the OH-H bond are 3.27 eV, 2.27 eV, 1.81 eV, respectively. Such high energy barriers hinder the dissociation of water. Strikingly, the water dissociation barrier at the Ni/NiO VAN interface is reduced to 1.53 eV on the NiO sites (Figure 5a), indicating that oxygen vacancies at the Ni/NiO interface can promote water dissociation, which is consistent with the NAP-XPS results. On the one hand, the generated OH^* will heal the oxygen vacancies and proceed the next reaction to produce oxygen. According to the previous reports,[61] the rate determining step of NiO for OER is the adsorption of OH^*, and we found that the presence of oxygen vacancies at the interface for Ni/NiO significantly enhance the adsorption of OH^*. Therefore, we conclude the underlying reason for the highest OER performance of Ni/NiO VAN, in comparison with individual NiO and Ni catalysts.

Previous reported works have proved that the optimal value of Gibbs free energy of H* (ΔG_{H^*}) is 0, where the adsorption and desorption of H* at the electrocatalyst can be well balanced for H_2 generation.[62] Therefore, the ΔG_{H^*} value of a catalyst could be reasonably utilized to judge the catalytic performance for HER (the closer to the ΔG_{H^*} value of 0, the better the HER activity). Based on that, we computed values ofΔG_{H^*} in order to analyze the optimum adsorption and recombination sites to form H_2. As shown in Figure 5b, the ΔG_{H^*} values of NiO sites near the interface and pure Ni are 0.66 eV and -0.58 eV, respectively, indicating that the adsorption of hydrogen on NiO sites near the interface is too weak, and the adsorption of hydrogen on pure Ni sites is too strong. However, the metallic Ni sites near the interface possessed the optimal ΔG_{H^*} value of -0.16 eV, suggesting that the metallic Ni sites near the interface show the best HER performance. To further explore the mechanism of boosted alkaline HER activity of the Ni/NiO electrocatalysts, the Bader charge analysis on Ni cations of Ni/NiO was conducted together with the average valence charge of Ni cations along the direction of the Ni/NiO heterointerface (Figure 5c). Combining with differential

https://engine.scichina.com/doi/10.1007/s11426-022-1326-2
http://chem.scichina.com/english

charge densities of the Ni/NiO electrocatalysts (the inset of Figure 5c), we can confirm the occurrence of charge transport nearby the Ni/NiO heterointerface, providing 0.33 e^- of charge transfer from metallic Ni phase to NiO phase. The electrons transfer between Ni and NiO may be driven by the difference in work function of NiO (5.2~5.6 eV) and that of metallic Ni (5.0~5.2 eV),[63, 64] *i.e.*, the Fermi level of NiO is lower than that of Ni. When Ni and NiO are brought into contacted, electrons in metallic Ni will spontaneously transfer to NiO. According to the d-band theory,[65] when the Ni atoms loss electrons and d band experiences a downward shift, more antibonding states of hydrogen are lower than the Fermi level, and hence weakens the affinity of Ni towards hydrogen. Therefore, the Ni sites near the interface exhibit more appropriate binding strength with H atoms, which improve the HER activity compared with pure metallic Ni. In view of the above results, we propose a mechanism for the enhanced HER in alkaline media on the Ni/NiO VAN electrocatalyst. As shown in Figure 5d, H_2O dissociation is assumed to occur on the NiO sites near the Ni/NiO VAN interface, where the oxygen vacancies reduce the dissociative energy barrier and promote to form chemisorbed OH_{ads} and H_{ads}. Then the produced H* will migrate to the metallic Ni sites for the further combination to form H_2.

4. Conclusion

In summary, we show that the Ni/NiO nanocomposite is an efficient catalyst for both alkaline HER and OER, due to a synergetic effect at Ni/NiO interface that significantly reduces the energy barrier for water dissociation and favors the formation of reactive key H* intermediates on the Ni side of the interface, and OH_{ads} on the NiO side of the interface. Different from previously reported Ni-based heterostructure catalysts, the Ni/NiO VAN shows a vertical aligned structure with abundant Ni/NiO heterointerfaces. Structural studies based on reciprocal mapping and EELS results show that the oxygen vacancies existing at NiO side of the interface lead to the formation of undercoordinated Ni cations. Experimental studies of water dissociation based on NAP-XPS and theoretical calculation based on DFT indicate that the existence of oxygen vacancies at the interface of Ni/NiO VAN promotes the water dissociation. On the other hand, the electron energetics of the interface tailors the ΔG_{H^*} of metallic Ni to an optimum value of -0.16 eV for an efficient H_2 evolution. This work provides a new method for the preparation of heterostructure electrocatalysts

with well-defined interfaces as a model system and reveals insights into the mechanism of Ni/NiO heterostructure for overall water splitting.

Acknowledgements

Kelvin H.L. Zhang is grateful for funding support by the National Natural Science Foundation of China (Grant No. 21872116). F. E. Oropeza and V. A. de la Peña O'Shea are grateful for the funding supported. by the EU (ERC CoG HyMAP 648319) and Spanish AEI (NyMPhA PID2019-106315RB-I00). Also, this work has been funded by the regional government of Comunidad de Madrid and European Structural Funds through their financial support to FotoArt-CM project (S2018/NMT-4367). Besides, Fundación Ramon Areces funded this work though ArtLeaf project. Kelvin H.L. Zhang also acknowledge the Sino-German Mobility Program (Grant No. M-0377). SuperSTEM is the National Research Facility for Advanced Electron Microscopy, funded from the Engineering and Physics Research Council (EPSRC). M.B. is grateful to the SuperSTEM Laboratory for microscope access, and to the School of Chemical and Process Engineering at the University of Leeds for a visiting associate professorship and financial support.

References

[1] Stamenkovic VR, Strmcnik D, Lopes PP, et al. *Nat mater*, 2017, 16: 57-69

[2] Wang H, Zhang KHL, Hofmann JP, et al. *J Mater Chem A*, 2021, 9: 19465-19488

[3] Montoya JH, Seitz LC, Chakthranont P, et al. *Nat mater*, 2017, 16: 70-81

[4] Wang C, Xu H, Gao F, et al. *Nanoscale*, 2019, 11: 18176-18182

[5] Zhu K, Shi F, Zhu X, et al. *Nano Energy*, 2020, 73:104761

[6] Jiang K, Liu B, Luo M, et al. *Nat commun*, 2019, 10: 1743

[7] Zhao D, Zhuang Z, Cao X, et al. *Chem Soc Rev*, 2020, 49: 2215-2264

[8] Hong WT, Risch M, Stoerzinger KA, et al. *Energy Environ Sci*, 2015, 8: 1404-1427

[9] Zou X, Zhang Y. *Chem Soc Rev*, 2015, 44(15): 5148-5180

[10] Wang C, Shang H, Li J, et al. *Chem Eng J*, 2021, 420:129805

[11] Li J, Zhou Z, Xu H, et al. *J Colloid Interf Sci*, 2022, 611:523-532

[12] Trotochaud L, Young SL, Ranney JK, et al. *J Am Chem Soc*, 2014, 136: 6744-6753

[13] Cui M, Ding X, Huang X, et al. *Chem Mater*, 2019, 31: 7618-7625

https://engine.scichina.com/doi/10.1007/s11426-022-1326-2
http://chem.scichina.com/english

[14] Yu R, Wang C, Liu D, et al. *Inor. Chem Front*, 2022, 9:3130-3137

[15] Zhao Y, Jin B, Zheng Y, et al. C. *Adv Energy Mater*, 2018, 8: 1801926

[16] Ji X, Lin Y, Zeng J, et al. *Nat commun*, 2021, 12: 1380

[17] Lagadec MF, Grimaud A. *Nat Mater*, 2020, 19: 1140-1150

[18] An L, Wei C, Lu M, et al. *Adv mater*, 2021, 33: 2006328

[19] Lao M, Rui K, Zhao G, et al. *Angew Chem Int,* 2019, 58: 5432-5437

[20] Wang L, Zhu Y, Zeng Z, et al. *Nano Energy*, 2017, 31:456-461

[21] Subbaraman R, Tripkovic D, Strmcnik D, et al. *Science*, 2011, 334:1256-1260

[22] Xu W, Zhu S, Liang Y, et al. *J MaterChem A*, 2018, 6: 5574-5579

[23] Yu F, Zhou H, Huang Y, et al. *Nat Commun*, 2018, 9: 2551

[24] Xie Y, Wang X, Tang K, et al. *Electrochim Acta*, 2018, 264:225-232

[25] Sun L, Luo Q, Dai Z, et al. *Coord Chem Rev*, 2021, 444:214049

[26] Shang X, Tang J-H, Dong B, et al. *Sustain Energy Fuels*, 2020, 4: 3211-3228

[27] Wang H, Fu W, Yang X, et al. *J Mater Chem A*, 2020, 8: 6926-6956

[28] Wei C, Sun S, Mandler D, et al. *Chem Soc Rev*, 2019, 48: 2518-2534

[29] Huang J, Wang H, Wang X, et al. *ACS Appl Mater Interfaces*, 2020, 12: 39920-39925

[30] Su Q, Zhang W, Lu P, et al. *ACS Appl Mater Interfaces*, 2016, 8: 20283-20291

[31] Cho S, Jang J-W, Li L, et al. *Chem Mater*, 2016, 28: 3017-3023

[32] Huang J, Wang X, Hogan NL, et al. *Adv Sci*, 2018, 5: 1800416

[33] Fan M, Zhang B, Wang H, et al. *Adv mater*, 2017, 29: 1606861

[34] Jiao Y, Hong W, Li P, et al. *Appl Catal B Environ*, 2019, 244:732-739

[35] Lei Y, Xu T, Ye S, et al. *Appl Catal B Environ*, 2021, 285:119809

[36] Wang J, Ge X, Shao L, et al. *Mater Today Energy*, 2020, 17:100436

[37] MacManus-Driscoll JL. *Adv Funct Mater*, 2010, 20: 2035-2045

[38] Wang X, Qi Z, Liu J, et al. *ACS Appl Mater Interfaces*, 2021, 13: 39730-39737

[39] Park S, Ahn H-S, Lee C-K, et al. *Phys Rev B*, 2008, 77: 134103

[40] Aidhy DS, Liu B, Zhang Y, et al. *Comput Mater Sci*, 2015, 99:298-305

[41] Biswas S, Husek J, Londo S, et al. *J. Phys Chem Lett*, 2018, 9: 5047-5054

[42] Jang WL, Lu YM, Hwang WS, et al. *EPL (Europhysics Letters)*, 2011, 96: 37009

https://engine.scichina.com/doi/10.1007/s11426-022-1326-2
http://chem.scichina.com/english

[43] Rodriguez JA, Hanson JC, Frenkel AI, et al. *J Am Chem Soc*, 2002, 124: 346-354

[44] Bao J, Zhang X, Fan B, et al. *Angew Chem Int*, 2015, 54: 7399-7404

[45] Hu C, Wang X, Yao T, et al. *Adv Funct Mater*, 2019, 29:1902449

[46] Uchimoto Y, Sawada H, Yao T. *J Power Sources*, 2001, 97-98:326-327

[47] Leapman RD, Grunes LA. *Phys Rev Lett*, 1980, 45: 397-401

[48] Sparrow TG, Williams BG, Rao CNR, et al. *Chem Phys Lett*, 1984, 108: 547-550

[49] Jeangros Q, Hansen TW, Wagner JB, et al. *Acta Mater*, 2014, 67:362-372

[50] Zhu Y, Li C, Wang Q, et al. *Appl Phys Lett*, 2019, 115: 143902

[51] Dickey EC, Dravid VP, Nellist PD, et al. *Microsc Microanal*, 1997, 3: 443-450

[52] Zhang JY, Li WW, Hoye RLZ, et al. *J Mater Chem C*, 2018, 6: 2275-2282

[53] Dudarev SL, Botton GA, Savrasov SY, et al. *Phys Rev B*, 1998, 57: 1505-1509

[54] Stevens MB, Enman LJ, Batchellor AS, et al. *Chem Mater*, 2016, 29: 120-140

[55] Stoerzinger KA, Wang L, Ye Y, et al. *J Mater Chem A*, 2018, 6:22170-22178

[56] Wang L, Stoerzinger KA, Chang L, et al. *ACS Appl Mater Interfaces*, 2019, 11: 12941-12947

[57] Stevens MB, Enman LJ, Batchellor AS, et al. *Chem of Mater,* 2017, 29: 120-140

[58] Qin F, Zhao Z, Alam MK, et al. *ACS Energy Lett*, 2018, 3: 546-554

[59] Shen Z, Zhuang Y, Li W, et al. *J Mater Chem A*, 2020, 8: 4407-4415

[60] Rao RR, Kolb MJ, Hwang J, et al. *J Phys Chem C*, 2018, 122: 17802-17811

[61] Fu G, Wen X, Xi S, et al. *Chem Mater*, 2018, 31: 419-428

[62] Morales-Guio CG, Stern L-A, Hu X. *Chem Soc Rev*, 2014, 43: 6555-6569

[63] Greiner MT, Helander MG, Wang Z-B, et al. *J Phys Chem C*, 2010, 114: 19777-19781

[64] Greiner MT, Lu Z-H. *NPG Asia Mater*, 2013, 5: e55

[65] Jiao S, Fu X, Huang H. *Adv Funct Mater*, 2022, 32: 2107651

https://engine.scichina.com/doi/10.1007/s11426-022-1326-2
http://chem.scichina.com/english

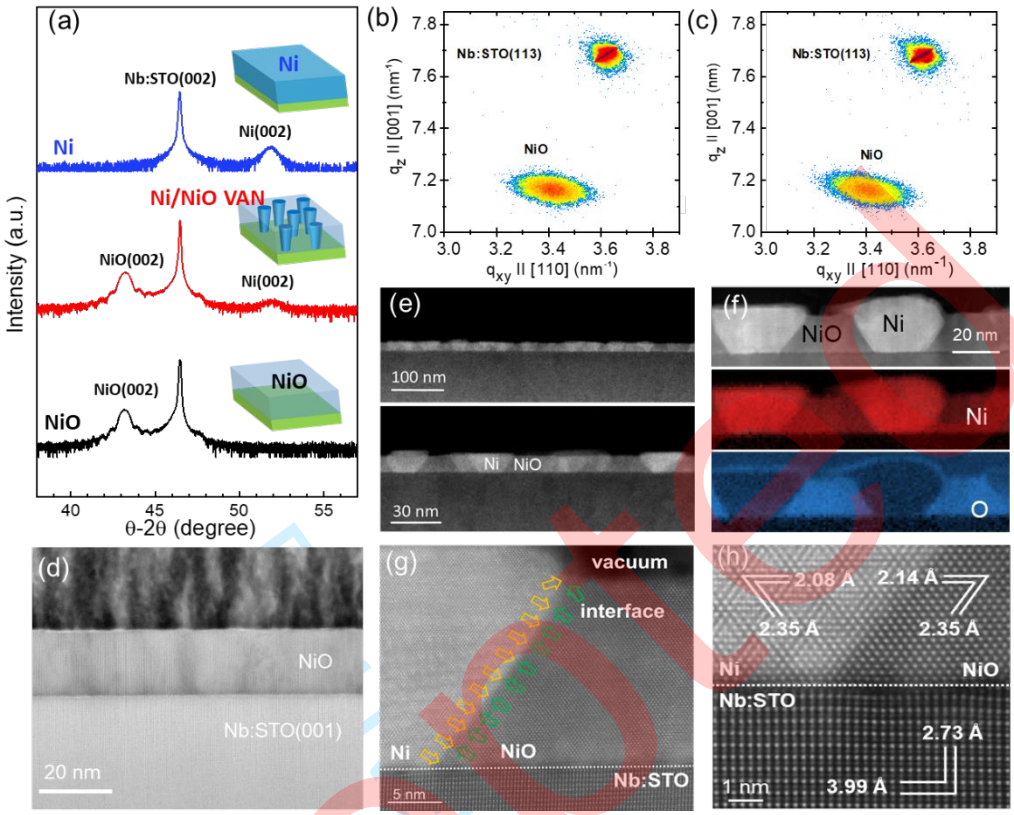

Figure 1 (a) XRD θ-2θ scans around (002) Bragg peaks for NiO, Ni/NiO VAN and Ni films grown on Nb:STO substrates. RSMs for NiO (b) and Ni/NiO VAN (c) around Nb:STO (113) reflection. Large-scale cross-sectional STEM images of Ni (d) and Ni/NiO VAN (e). (f) The HAADF-STEM image and corresponding EDX elemental maps of Ni/NiO VAN. (g) and (h) Cross-sectional HAADF-STEM micrograph at the Ni/NiO interface.

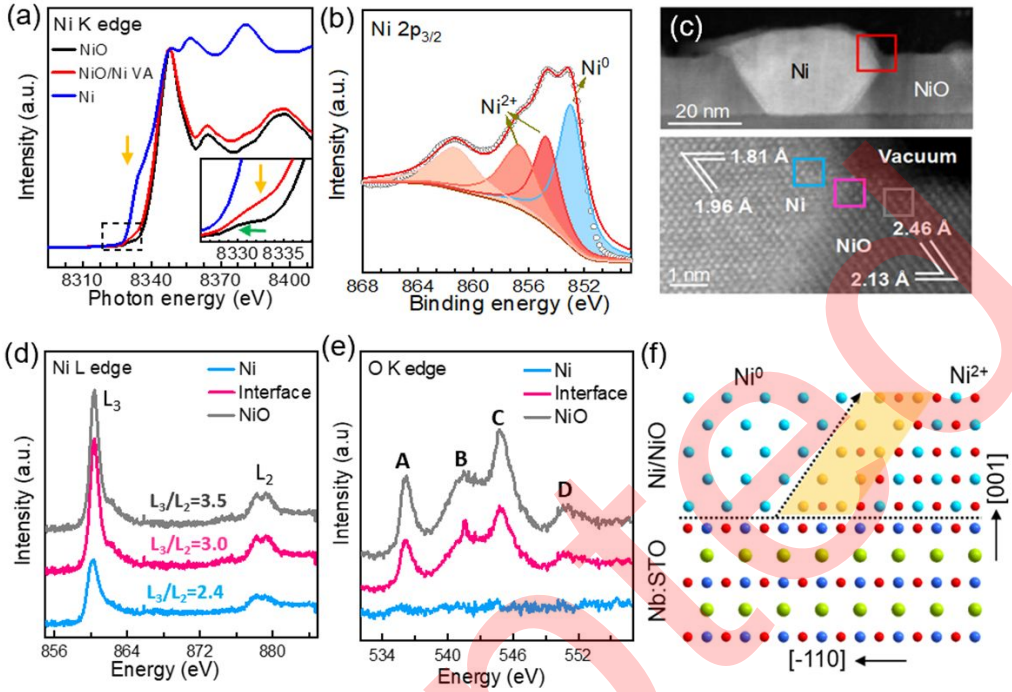

Figure 2. (a) Ni-K edge XAS of NiO, Ni/NiO VAN and Ni. (b) High resolution XPS spectra of Ni $2p_{3/2}$ for Ni/NiO VAN. (c) STEM images of Ni/NiO VAN, indicating the selected region for EELS measurement. Ni-L edge (d) and O-K edge (e) EELS of Ni/NiO VAN. (f) Schematic diagram of Ni/NiO heterostructure with oxygen vacancies at the interface.

https://engine.scichina.com/doi/10.1007/s11426-022-1326-2
http://chem.scichina.com/english

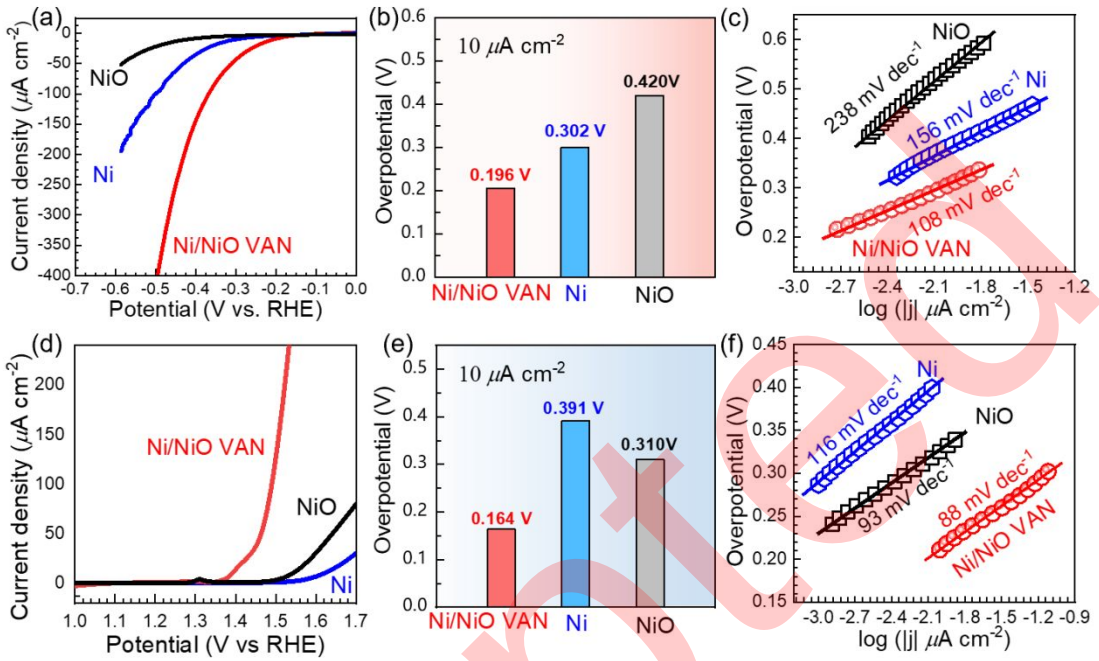

Figure 3. (a) LSV curves of NiO, Ni/NiO VAN and Ni electrodes for HER. (b) Overpotentials to reach a current density of 10 μA cm^{-2}. (c) The Tafel slopes for HER. (d) LSV curves of NiO, Ni/NiO VAN and Ni electrodes for OER. (e) Overpotentials to reach a current density of 10 μA cm^{-2}. (f) The Tafel slopes for OER.

https://engine.scichina.com/doi/10.1007/s11426-022-1326-2
http://chem.scichina.com/english

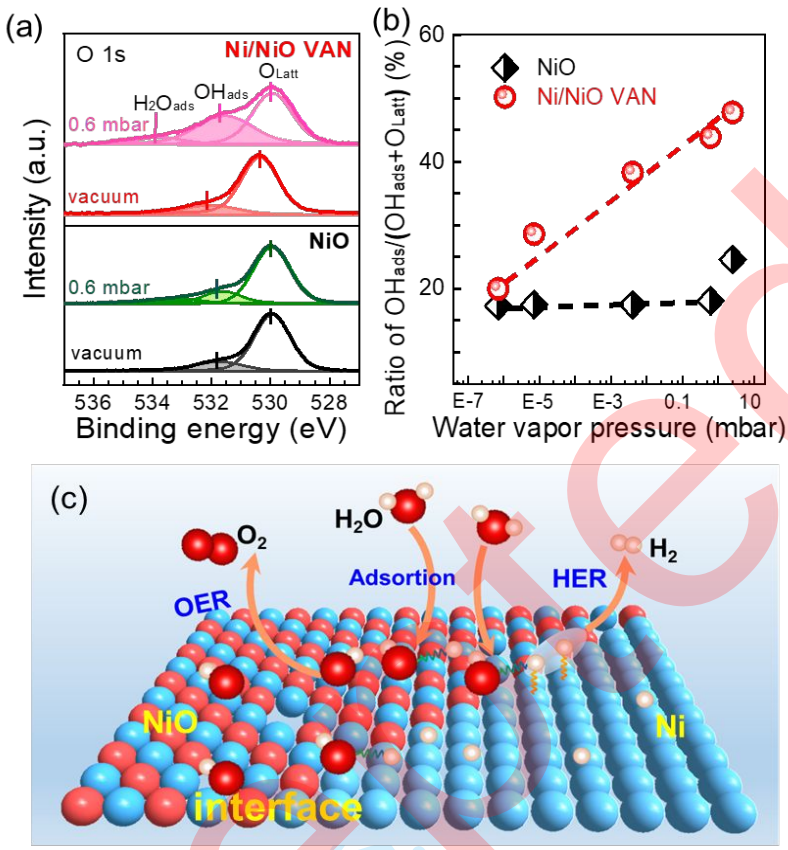

Figure 4. (a) O 1s NAP-XPS spectra of NiO, Ni/NiO VAN under different water vapor pressures. (b) Plots of the percentage of adsorbed hydroxyl as a function of water vapor pressure. (c) Schematic illustration of the enhanced water dissociation mechanism by oxygen vacancies at the Ni/NiO interface.

https://engine.scichina.com/doi/10.1007/s11426-022-1326-2
http://chem.scichina.com/english

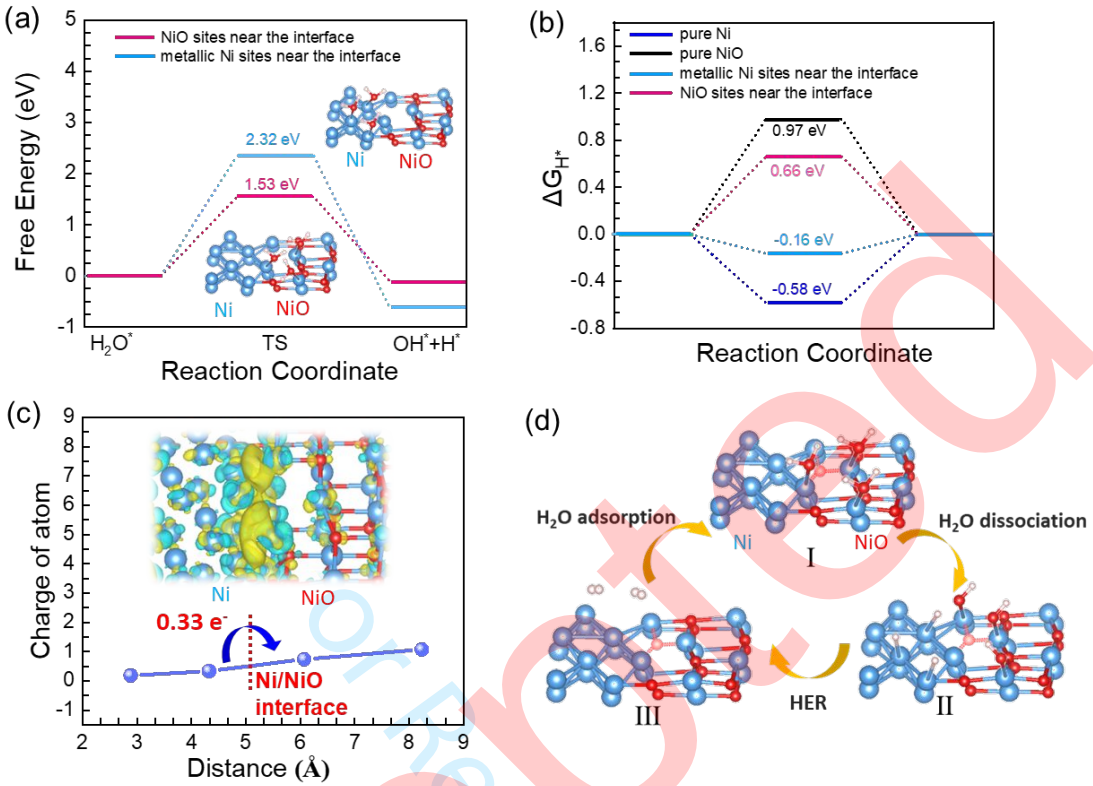

Figure 5. (a) Calculated energy barriers of water dissociation kinetics of the metallic Ni sites near the interface and NiO sites near the interface. (b) Calculated Gibbs free energy of H on pure Ni, pure NiO, the metallic Ni sites near the interface and NiO sites near the interface, respectively. (c) Bader charge analysis of Ni cations along the direction of Ni/NiO VAN via a heterointerface. The inset in (c) is the differential charge density of a Ni/NiO heterointerface. Yellow and blue delocalized sections represent the increase and decrease of electron density, respectively. (d) Schematics of the HER pathway on the Ni/NiO VAN electrocatalysts in alkaline media.

https://engine.scichina.com/doi/10.1007/s11426-022-1326-2
http://chem.scichina.com/english

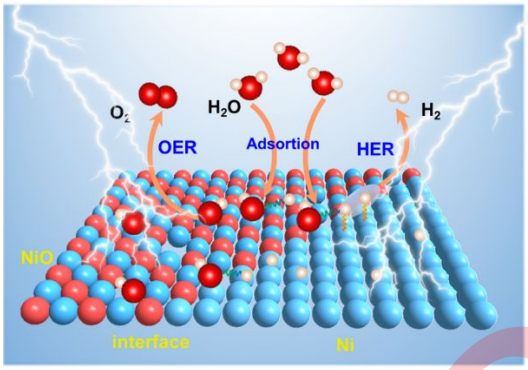

Graphical abstract picture.

https://engine.scichina.com/doi/10.1007/s11426-022-1326-2
http://chem.scichina.com/english

Supporting information

Vertically Aligned Ni/NiO Nanocomposites with Abundant Oxygen Deficient Hetero-interfaces for Enhanced Overall Water Splitting

Hongxia Wang[1#], Meiyan Cui[2#], Gaoliang Fu[1,3], Jiaye Zhang[1], Xingyu Ding[1], Irene Azaceta[4], M. Bugnet[5,6,7], Demie M. Kepaptsoglou[4,5], Vlado K. Lazarov[4], Victor de la Peña O'Shea[8], Freddy E. Oropeza[8*], and Kelvin H. L. Zhang[1*]

[1]*State Key Laboratory of Physical Chemistry of Solid Surfaces, College of Chemistry and Chemical Engineering, Xiamen University, Xiamen 361005, P. R. China*

[2]*State Key Laboratory of Structural Chemistry, Fujian Institute of Research on the Structure of Matter, Chinese Academy of Sciences, Fuzhou 350002, P. R. China*

[3]*Henan Provincial Key Laboratory of Nanocomposites and Applications, Institute of Nanostructured Functional Materials, Huanghe Science and Technology College, Zhengzhou, Henan 450006, China*

[4]*Department of Physics, University of York, Heslington, York, YO10 5DD, U. K.*

[5]*SuperSTEM Laboratory, SciTech Daresbury Campus, Daresbury WA4 4AD, United Kingdom*

[6]*School of Chemical and Process Engineering, Univeristy of Leeds, Leeds LS2 9JT, United Kingdom*

[7]*Univ Lyon, CNRS, INSA Lyon, UCBL, MATEIS, UMR 5510, 69621 Villeurbanne, France*

[8]*Photoactivated Processes Unit, IMDEA Energy Institute, Parque Tecnológico de Móstoles, Avda. Ramón de la Sagra 3, 28935 Móstoles, Madrid, Spain.*

#Equal Contribution

Email: freddy.oropeza@imdea.org; kelvinzhang@xmu.edu.cn

Computational methods:

Spin polarized DFT calculations were performed using the Vienna ab initio simulation package (VASP).[1, 2] The generalized gradient approximation proposed by Perdew, Burke, and Ernzerhof (GGA-PBE) is selected for the exchange-correlation potential.[3] The pseudo-potential was described by the projector-augmented-wave (PAW) method.[4] The geometry optimization is performed until the Hellmann–Feynman force on each atom is smaller than 0.03 $eV \cdot Å^{-1}$. The energy criterion is set to 10^{-6} eV in iterative solution of the Kohn-Sham equation. Ni(001) and NiO(001) slab models were used for adsorption studies. For the study of NiO/Ni heterojunction, NiO(-100) and Ni(100) surface were built together and optimized, and the (001) surface of the heterojunction was cleaved with 12 Å vacuum above the model. The bottom two layers of atoms were fixed for all optimizations. Nudged elastic band method (NEB)[5, 6] was used to search for transition state structures.

https://engine.scichina.com/doi/10.1007/s11426-022-1326-2
http://chem.scichina.com/english

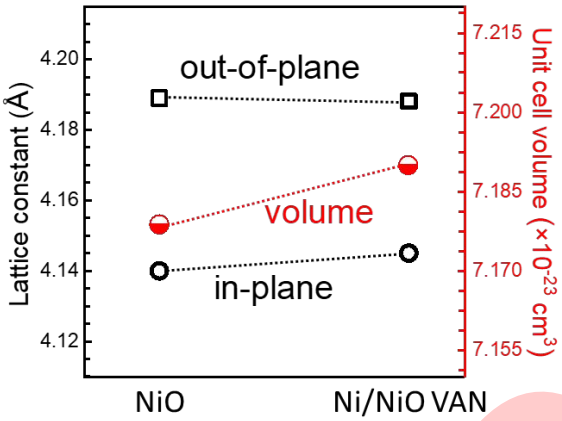

Figure S1. The out-of-plane lattice parameters, in-plane lattice parameters and unit cell volumes of the NiO and Ni/NiO VAN extracted from RSMs.

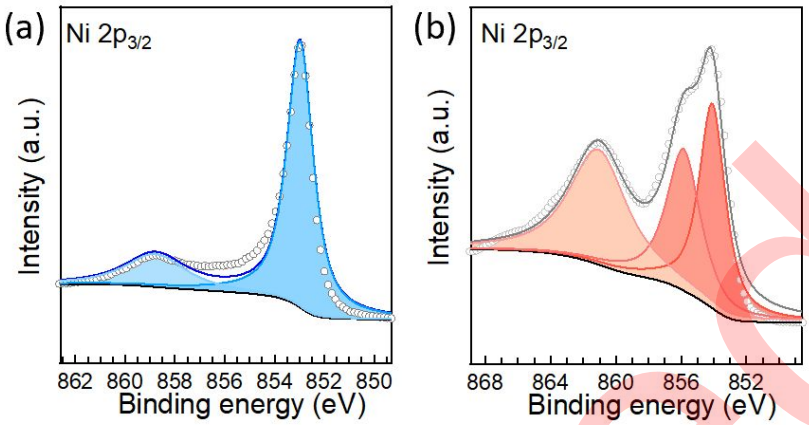

Figure S2. High resolution XPS spectra of Ni $2p_{3/2}$ for (a) Ni and (b) NiO.

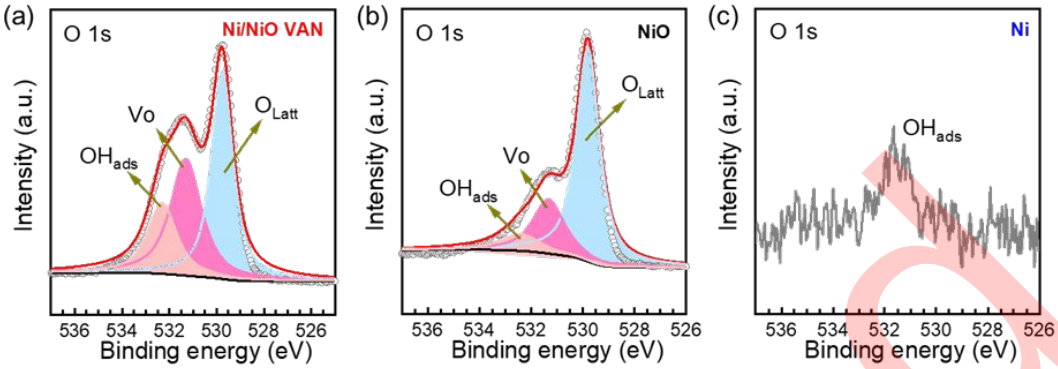

Figure S3. High resolution XPS spectra of O 1s for (a) Ni/NiO VAN, (b) NiO, and (c) Ni.

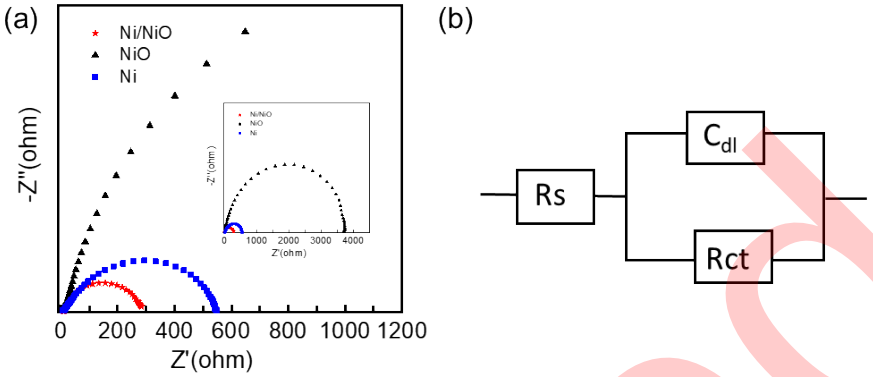

Figure S4. Nyquist plots of the electrochemical impedance spectroscopy at the potential of -0.4 V vs RHE. (b) The equivalent circuit image, R_s, R_{ct} and C_{dl} mean the electrolyte resistance, charge transfer resistance and electrical double-layer capacitance, respectively.

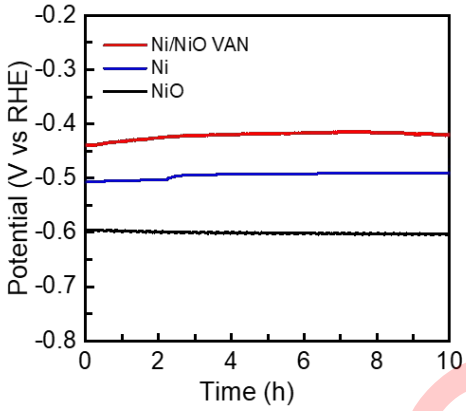

Figure S5. Stability curves measured at constant current density of -20 μA cm^{-2} in 0.1 M KOH.

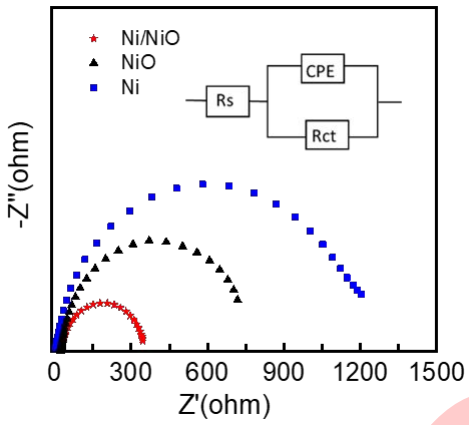

Figure S6. Nyquist plots of the electrochemical impedance spectroscopy at the potential of 1.6 V vs RHE. The inset is the equivalent circuit.

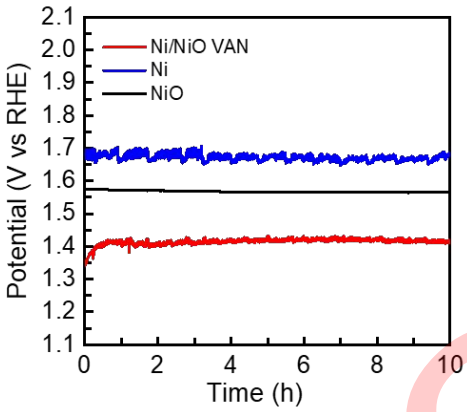

Figure S7. Stability curves measured at constant current density of 20 μA cm^{-2} in 0.1 M KOH.

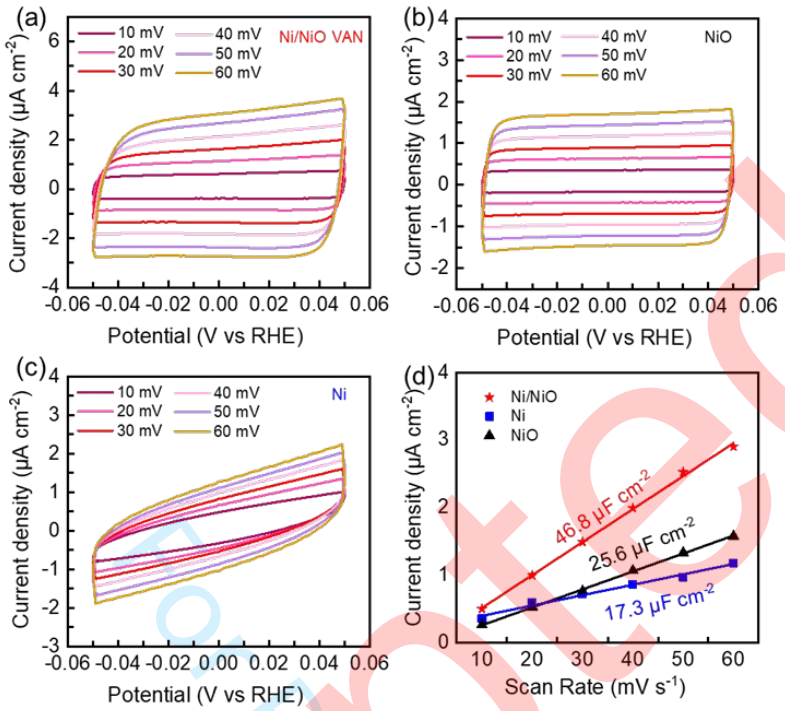

Figure S8. CV curves of (a) Ni/NiO VAN, (b) Ni, and (c) NiO at different scan rates from 10 to 60 mV s^{-1}. (d) Liner fitting of the capacitive currents of the catalysts versus scan rate.

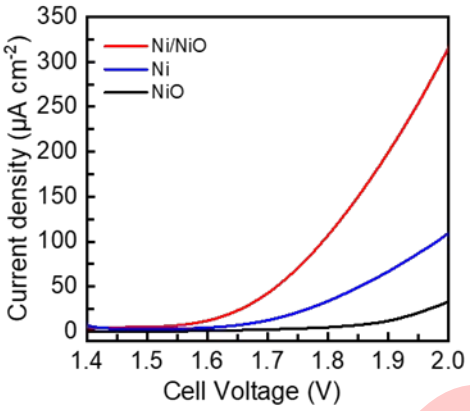

Figure S9. LSV curves of water electrolysis with a two-electrode configuration in 0.1 M KOH.

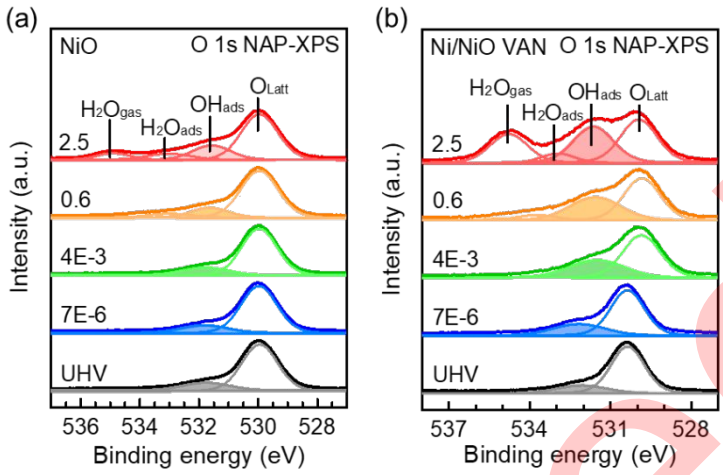

Figure S10. O 1s NAP-XPS spectra of NiO, Ni/NiO VAN under different water vapor pressures.

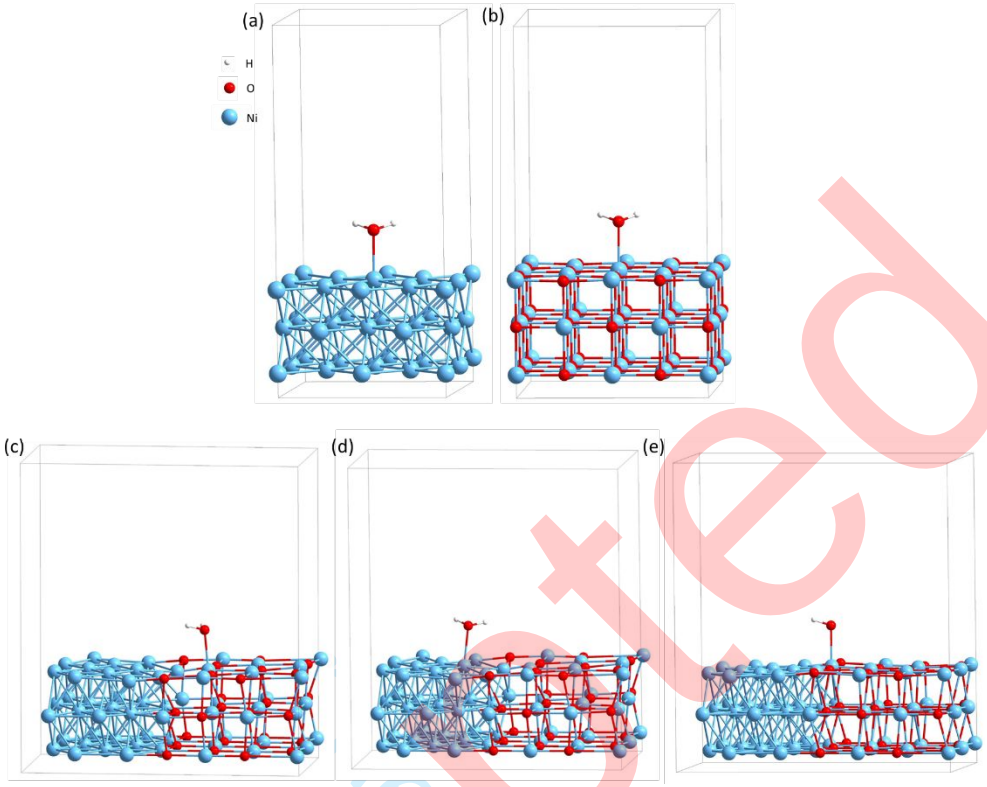

Figure S11. Atomic structure of H_2O adsorbed on: (a) Ni (001), (b) NiO (001), (c) metallic Ni sides near the interface in Ni/NiO (001) and (d) NiO sites near the interface in Ni/NiO (001), and (e) NiO sites near the interface in w/o-Ni/NiO (001).

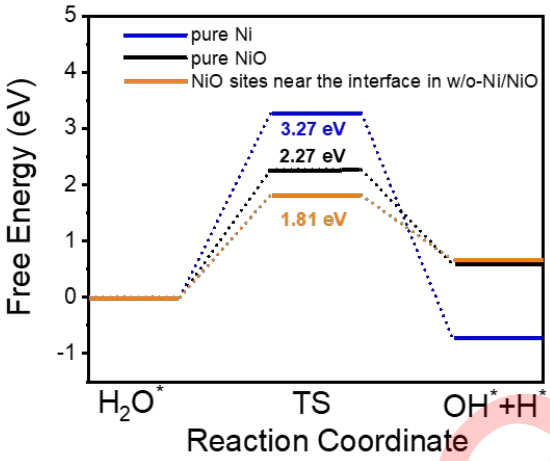

Figure S12. Calculated energy barriers of water dissociation kinetics of pure Ni (001), pure NiO (001), and NiO sites near the interface in w/o-Ni/NiO (001).

References

[1] Kresse G, Furthmüller J. *Comp Mater Sci*, 1996, 6: 15-50

[2] Kresse G, Furthmüller J. *Phys Rev B*, 1996, 54: 11169-11186

[3] Perdew JP, Burke K, Ernzerhof M. *Phys Rev B*, 1996, 77: 3865-3868

[4] Blöchl PE. *Phys Rev B*, 1994, 50: 17953-17979

[5] Sheppard D, Xiao P, Chemelewski W, et al. *J Chem Phys*, 2012, 136: 074103

[6] Sheppard D, Henkelman G. *J Comput Chem*, 2011, 32(8): 1769-1771